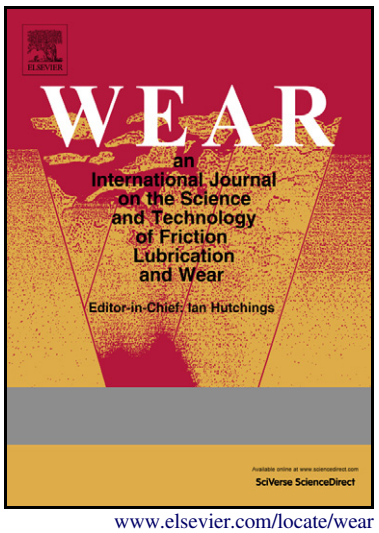

www.elsevier.com/locate/wear

Simultaneous observation of cavitation structures and cavitation erosion

Martin Petkovšek, Matevž Dular

PII: S0043-1648(13)00128-2
DOI: http://dx.doi.org/10.1016/j.wear.2013.01.106
Reference: WEA100611

To appear in: *Wear*

Received date: 6 August 2012
Revised date: 10 January 2013
Accepted date: 22 January 2013

Cite this article as: Martin Petkovšek and Matevž Dular, Simultaneous observation of cavitation structures and cavitation erosion, *Wear,* http://dx.doi.org/10.1016/j.wear.2013.01.106

Simultaneous observation of cavitation structures and cavitation erosion

Martin Petkovšek
Laboratory for Water and Turbine Machines
Faculty of Mechanical Engineering
University of Ljubljana
Askerceva 6
1000 Ljubljana
SI-Slovenia

Matevž Dular (corresponding author)
Laboratory for Water and Turbine Machines
Faculty of Mechanical Engineering
University of Ljubljana
Askerceva 6
1000 Ljubljana
SI-Slovenia

E-mail: matevz.dular@fs.uni-lj.si
Phone: +386 1 4771 453
Fax: +386 1 2518 567

Abstract

Despite a large ensemble of works on the relationship between the macroscopic cavitation structures and their erosive potential a study that would link individual cavitation events with specific damage has not yet been made.

In the present study we attached a thin aluminum foil to the surface of a transparent Venturi section using two sided transparent adhesive tape. The surface was very soft – prone to be severely damaged by cavitation in a very short period of time. Using two high speed cameras we simultaneously recorded cavitation structures and the surface of the foil.

Analysis of the results revealed that damage only occurs at cavitation cloud collapse, that the size of the cloud and it distance from the wall at collapse do not influence the extent of the damage and that an irregular or "broken" type of cavitation cloud causes the most damage to the foil. Also and probably the most important of all the study shows the sequence where one can see the separation and the collapse of cavitation cloud and the corresponding appearance of cavitation erosion.

Key words: Cavitation, erosion, aluminum foil, high speed camera, Venturi section

1 Introduction

It is well known that cavitation can severely damage solid walls by removing material from the surface – almost a century ago Rayleigh [1] introduced the problem of cavitation erosion of the ship propellers. The phenomenon is complex as it includes both hydrodynamic and material aspects [2].

From a hydrodynamic point of view, vapour structures are produced in the low pressure regions and are convected downstream. The difference in pressures inside and the outside of the fixed cavity causes the deviation of surrounding streamlines towards the solid wall. They then separate into outer flow, which reattaches to the wall and to the re-entrant jet, which causes a new separation of the cavitation cloud [2].

Cavitation structures carry a significant amount of potential energy [3] and can, at their collapse, emit pressure waves of magnitude of several MPa [4]. Yet it seems that the cavitation cloud collapse itself cannot be the direct cause of erosion as its energy is not concentrated enough. Hence another or a number of other processes must be involved in the process of damage occurrence – some even question the importance of the cavitation cloud collapse – for example Chen & Israelachvili [5] suggested that the erosion occurs during cavity formation and not during its collapse.

As already mentioned, Hammitt [3] postulated that cavitation damage occurs once the potential energy contained in a cavity exceeds a certain damage threshold. This threshold is essentially a function of the material properties on which the erosive action takes place, and not of the type of cavitation [6]. Currently the most widely accepted explanation of the phenomenon is that the potential energy contained in a macro cavity (cavitation cloud) is transformed into the radiation of acoustic pressure waves, and further on into the erosive power contained of the micro-scale cavitation structures or single bubbles that implode in the vicinity of the material boundaries. The approach, known as the "multiscale energy cascade", was first used by Fortes-Patella et al. [7] and Bark et al. [8] to explain the damage occurrence.

Despite a large ensemble of works on the relationship between the macroscopic cavitation structures and their erosive potential [9-13], a study that would link individual cavitation events (one cavitation collapse) with specific damage (single pit or a group of pits) has not yet been made. This is mainly due to the difficulty of the measurements – on one hand cavitation is a fast phenomenon where clouds separate and collapse at a rate of 10 to1000 times per second and on the other hand cavitation erosion is a relatively slow process– for 316L stainless steal the pitting rate lies between 1 and 100 pits/cm^2/s [14]. Also, it is difficult, if not impossible, to see the surface that is being damaged as cavitation bubbles and clouds surround it.

A study where cavitation structures and cavitation erosion would be simultaneously observed is also of a great interest for evaluation and further development of cavitation erosion prediction models (7, 15-18]. This is a major issue since CFD predictions of cavitation erosion [7, 19] usually base on a very short flow simulation time and rely on erosion data obtained after a long exposure to cavitating flow (for example 38 ms of flow simulation time against erosion data obtained after 1 hour exposure to cavitation [19]).

Quantification the cavitation erosive aggressiveness is a major scientific issue. Only very recently some methods for measuring the pressure peaks caused by bubble implosions were developed [20]. Still the most common method is the usage of soft metal (aluminum or copper) or paint coating of the submerged body as a sensor [21–25]. The erosion evaluation method, using the number, distribution and shape of the pits caused by bubble implosions gives us a relatively detailed knowledge of the flow aggressiveness.

In the present study we attached a thin aluminum foil to the surface of a transparent Venturi section using two sided transparent adhesive tape. The surface appeared polished and was very soft – prone to be severely damaged by cavitation in a very short period of time. Using two high speed cameras we simultaneously recorded cavitation structures (from the side view) and the surface of the foil (from the bottom view).

Analysis of the results revealed that damage only occurs at cavitation cloud collapse, that the size of the cloud and it distance from the wall at collapse do not influence the extent of the damage and that an irregular or "broken" type of cavitation cloud causes the most damage to the foil. Also and probably the most important of all the study shows the sequence where one can see the separation and the collapse of cavitation cloud and the corresponding appearance of cavitation erosion.

2 Experimental set-up

Cavitation tests were performed in a cavitation tunnel at the Laboratory for Water and Turbine Machines, University of Ljubljana.

2.1 Experimental set-up and the Venturi geometry

The basic geometry was a 10 mm wide Venturi section with a converging angle of 18º and diverging angle of 8º (Fig. 1). The throat dimensions were $10\times10\text{mm}^2$. The test section was made out of transparent plexi glass so that observation from all directions was made possible. Similarly the Venturi section was made out of ordinary glass which is, like plexi glass, transparent but also much more rigid what makes cavitation erosion on its much more aggressive.

The cavitation tunnel (Fig. 2) has a closed circuit what enables to vary the system pressure and consequently the cavitation number (Eqn. 1), which is defined as the difference between the reference pressure p_∞ (measured 200mm upstream of the Venturi throat) and vapour pressure p_v (at system temperature T_∞) divided by the dynamic pressure (defined by the fluid density ρ and the flow velocity v):

$$\sigma = \frac{p_\infty - p_v}{\frac{1}{2}\rho v^2} \qquad (1)$$

Decreasing the cavitation number results in higher probability in cavitation occurrence or leads to an increase of the magnitude of the already present cavitation.

Circulation of water is obtained with a 4.5 kW pump (1) that enables the variation of the rotation frequency in order to set the flow rate. At the pump delivery, a tank partially filled with the circulation water (2) is used for water heating (if necessary) and for damping the periodical flow rate and pressure fluctuations due to the passage of the pump blades. Cavitation and its effects are observed in a transparent plexi glass test section (3). The tank downstream of the test section (4) is used for cooling of the circulation water – cooling water flows inside the tank in a secondary loop which is connected to cold (14°C) tap water. Two valves (5 and 6) are installed upstream and downstream of the test section. These enable easy and fast disconnection of the test section from the main loop and also allow additional control of the flow rate. The volume flow rate is measured by electromagnetic flow meter (7) ABB WaterMaster V (DN 40) with a 2% uncertainty on measurements. Temperature is obtained with a type K thermocouple (8) which is directly in contact with the circulation water. The reference pressure is measured 200 mm upstream from the Venturi type section with a ABB 266AST pressure transducer (9). The uncertainty of the measurements was 8 mbar. The pressure in the test rig is adjusted in the partially filled tank (2) connected to a compressor (10) and a vacuum pump (11), which enables to vary the absolute pressure in this tank between 0.1 bar and 6 bar.
The quality of water can significantly influence the erosion rate – lower gas content results in more aggressive cavitation [26]. To increase the aggressiveness of cavitation the water was degassed by running the test rig at a low pressure for 30 minutes. In order to assure repeatable measurements the quantity of the dissolved gases was measured by the Van-Slyke method [27] – according to [28, 29] the increase of the dissolved gases is proportional to the increase of the cavitation nuclei content. The gas content of 15 mg of gases per liter of water was constantly measured.

The precisions of the pressure and velocity measurements result in a mean uncertainty of 3% for the cavitation number.

The idea was to obtain sufficient damage in a very short period of time (1 to 2 seconds). Setting the flow velocity and the cavitation number by gradually adjusting the pressure and the flow rate was therefore made impossible (the foil would be severely damaged before we could start the image acquisition). To set the operating conditions, first the test rig pressure was set to a desired value

(454000 Pa, absolute pressure), then the valve upstream of the test section (5) was closed and the pump was switched on to a determined rotating frequency. As the valve (5) was rapidly opened the velocity increased from 0 to 24.7 m/s (the final Reynolds number based on the height of the Venturi throat was: Re = 247000) in about 0.05 s. Figure 3 shows the evolution of the mean attached cavitation length during the experiment as a function of time. In the images of cavitation, the flow is from the right to the left, the bottom of the Venturi in on the top of the image and the region of interest extends over approximately 20x100 mm (see also Fig 5).

The desired operating conditions are achieved about 0.05 s after the first bubbles are seen. The cavitation than rapidly grows and exhibits the first cloud separation just 0.02 s after it first appeared. Looking at the transient one would expect the pitting rate to change during the first 0.1 s. Yet this proved to be practically unmeasurable (Figs. 8, 9 and 11) since the transition phase is very short (only a few cloud separations and collapses occur during the transient).

2.2 Aluminum foil as an erosion sensor

The idea of the experiment was to simultaneously record images of cavitation structures and cavitation erosion. The upper side of the foil is covered by vapour structures that obstruct the view, hence one needs to look at the foil from the bottom side to see the damage. Consequently the whole test section had to be made of transparent material and equally important the foil had to be thin enough so that the cavitation damage which occurs on the side exposed to cavitation was also visible on the other side. Furthermore the damage needs to occur very rapidly – if possible at every cavitation cloud collapse so that one is able to record it by high speed cameras.

We have chosen 10 μm thick aluminum foil and attached it to a Venturi section by a transparent two sided adhesive tape with thickness of 50 μm (Fig. 4). The Venturi section itself had to be made out of ordinary glass which is more rigid than the plexi glass – if the former was used practically no damage was recorded even after a long exposure to cavitation (1 hour).

The Venturi section which was prepared in the same way as for the experiments was tested for hardness - a value of only 0.4 HB was repeatably obtained.

2.3 Image acquisition

Two cameras were used in the experiment. For observation of the aluminum foil we used a high speed camera Fastec Imaging HiSpec4 2G mono which can capture images at 523 fps at 3Mpixel resolution. For capturing the cavitation structures from the side view we used high speed camera Motion Blitz EoSens mini 1 which can record at 506 fps at 1Mpixel resolution. For the present experiment the cameras were synchronized and recorded at 6000fps at a reduced resolution.

The regions of interest for the two cameras can be seen in Fig. 5. Images of cavitation were recorded at a resolution of 672×135 pixels and the images of the foil at a somewhat higher resolution of 1280×150 pixels. One pixel in the images of cavitation structures corresponds to 0.133 mm (the region of interest extends over approximately 90×18 mm). For the images of the foil the pixel size is 0.062 mm (the region of interest extends over 80×10 mm and begins 5 mm downstream of the throat of the Venturi).

2.4 Damage evaluation

Since we are observing the foil with a camera only the surface of the damaged area can be accurately measured. The volume of the pits could only be estimated using rough assumptions [30].
For evaluation we used an approach that combines several evaluation procedures used before (11, 31, 32).
We evaluated the images in pairs – the image at the time t was subtracted from the image at time $t+\Delta t$, thus eliminating most of the surface and illumination imperfections. Then we employed the pit-count method [11] which determines the pits from the darker regions in an image, while the brighter area is assumed to be undamaged surface – from each image pair we obtained the number and the area of newly appeared pits.

The pit-count method gives a distribution of the number and the area of the pits and consequently, the distribution of the magnitude of cavitation erosion on the surface. We can also determine the distribution of the size of the pits. Since we were comparing pairs of two successive images we were also able to consider the possibility of pit overlapping (Fig. 6).

Images of the aluminum foil were treated as matrixes with i×j (1280×150) elements ($A(i,j) \in \{0,1,\ldots 255\}$) with values which can range from 0 (black) to 255 (white).
Erosion was evaluated in image pairs: image matrix at time $t+\Delta t$ was subtracted from image matrix at

time t (B(i,j,t)= A(i,j,t) - A(i,j,t+Δt)). This way a new matrix B was obtained. When the matrix element B(i,j) did not change between times t and t+Δt its value was 0 (B(i,j,t)=0). When change occurred the value was B(i,j,t)≠0. Since small changes could be present due to insignificant changes in illumination, vibration etc., damage was only considered when a certain change threshold was exceeded (B(i,j,t)>12; this corresponds to more than 5% of decrease in brightness – pits always appeared as dark regions). The number of the pits, their size and overall damaged area could then be easily determined.

3 Results

Figure 7 shows a sequence where cavitation structures and the images of the aluminum foil are presented. The sequence starts 0.1045s after the cavitation first appears (some damage can already be seen from previous collapses) and shows one cavitation cloud collapse and rebound (last image). The flow is from the right to the left, flow velocity in the throat is v=24.7m/s and cavitation number is σ=1.48.

Cavitation cloud shedding begins with the cloud separation from the attached cavity. It then travels with the flow and collapses in a higher pressure region downstream. At the rear part of the attached cavity a back flow (re-entrant jet) forms that eventually cuts the cavity in two and causes a new separation of the cloud [2].

We can see that pits form immediately after the collapse of the cavitation cloud (in the present sequence we have two clouds that collapse at t=0.10500 s and 0.10517 s, respectively). It can also be seen that the region where most of the pitting occurs corresponds to the position of the cloud collapse. It is interesting to see that not a single pit forms but rather a cluster of them. We hypothesize that the shock wave from the cavitation cloud collapse interacted with several bubbles which were present in the vicinity of the wall (aluminum foil).

It also points to the idea of the cascade explanation of cavitation erosion process, which states that the damage occurrence is a consequence of a chain of events – for example according to Fortes-Patella et al. [7]: cavitation cloud collapse, shock wave generation, spherical micro-bubble collapse and shock emission and finally pit formation. Or in the case of Dular et al. [11]: cavitation cloud collapse, shock wave generation, micro-jet collapse of bubble in the vicinity of the wall, and finally the damage occurrence due to high velocity liquid jet impact to the solid surface.

In Fig. 8 the damage to the aluminum foil after different times of exposure to cavitation is shown. The

flow is from right to the left (the right boundary of the images lies 5 mm downstream of the throat of the Venturi – see also Fig. 7).

Within the first 0.1 seconds of exposure to cavitation the foil sustained damage in two regions – a few pits about 30 mm downstream of the throat of the Venturi and somewhat more damage further down – about 55 mm from the throat. Later on the damage in the region close to the throat of the Venturi (at the right side of the images) does not increase at the same rate as in the region downstream. This is due to the procedure of the experiment – as the valve was opened the velocity increased from 0 to 24.7 m/s and the cavitation grew (Fig. 3). Since cavitation was small at the beginning also the damage was not that severe and it occurred in the region close to the throat (<35mm) – nevertheless since the cavitation rapidly grows and exhibits cloud separation just 0.02 s after it first appears, a deviation of the pitting rate during the first 0.1 s is practically unmeasurable. When the cavitation fully develops (after 0.05 s, Fig. 3) cloud collapses occur further downstream and the region near the Venturi throat (the first 20 mm) remains almost intact until the end of the measurement. The damage, in the region where the clouds collapse, increases gradually till the end of the experiment what corresponds to the findings of Osterman et al. [33], who measured linear trend during the incubation period.

We can plot the number of pits and the whole damaged area as a function of time. When we calculate the two parameters we also need to consider the possibility of overlapping of the pits. At every time two successive images of the damaged surface are compared, this way it is possible to determine if a single damaged region corresponds to more than one pit. Also in the right diagram (Fig. 9) instances where the cloud collapse occurred are noted.

From the left diagram in Fig. 9 one can see that the pitting rate does not vary significantly during the length of the experiment (apart from the first 0.02 s when the cavitation was not fully developed). Both the area and the number of pits grow linearly at about 20 mm^2/s and 2200 pits/s (or as a function of the analyzed area: 2.5 $mm^2/cm^2/s$ and 275 $pits/cm^2/s$), respectively. More interesting is the diagram on the right. When we close in to a detail we see that the evolution is in fact not linear but rather stepwise. The dotted lines denote the instances of cavitation cloud collapse. It is obvious that they relate perfectly to the appearances of the damage. The cloud collapse is not instantaneous, hence the damage appears both prior and after the main cloud implosion. Still, this confirms the hypothesis that the cloud collapse is a needed condition for the erosion appearance as the foil does not sustain any damage during the rest of time.

The diagrams in Fig. 10 show the average pit size during the experiment (left) and histograms of pit size distribution (middle) and the contribution to the whole damaged area of the pits of a specific size (right) by the end of the experiment.

It is interesting to see that the pit size does not vary significantly during the experiment. The average area of the pit remains almost constant at about 0.009 mm^2, what corresponds to a circular pit with a diameter of 0.11 mm. The temporal variations of the size are below the one pixel resolution. This gives another proof of the linear increase of the damage during the incubation period. More importantly the result also implies that the small imperfections of the pitted surface did not influence the pitting later on.

The left histogram shows that the majority of the pits are small (area < 0.05 mm^2) – only a few large pits (area > 0.05 mm^2) form during the experiment. Also we see, from the right histogram, that larger pits do not contribute significantly to the whole damaged area.

Similarly to the acoustic cavitation where Dular & Osterman [31] reported that the pits tend to form erosion clusters this was also observed in the present experiment. One can see that area of the foil that was damaged by the erosion extends to about 12.7 mm^2 (Fig. 8 at 1.483 s), yet the whole area of the pits sums up to 28.8 mm^2 (maximal value of the in Fig. 9, left). This implies a very high level of overlapping. One can examine the clustering in detail by plotting a histogram that shows the number of deformations that formed a single pit as seen by the end of the experiment (Fig. 11).

We can see that the majority of the pits (83%) damaged the virgin material – they are formed during a single cavitation event. However, in very rare cases (10 pits), a single pit was damaged more than 10 times by the end of the experiment. Such a high level of very local overlapping or clustering can probably be related to the very soft, and therefore specific, nature of the material.

One also needs to question the repeatability of the measurements. Figure 12 shows the number of pits and integral damage extent as a function of time for 4 additional experiments which were conducted at the same conditions as the first one (v=24.7m/s, p=454000 Pa, σ=1.48). Also the damage after 0.8 s exposure to cavitation for all 5 cases are presented.

Cavitation is a random phenomenon, hence large discrepancies between the experiments were expected (for example Test no. 2 between 0.2 and 0.6 s). However both, the damaged surface area and the distribution of pits after the termination of the experiment, do not significantly differ from one experimental run to another. We can conclude that the properties of the aluminum foil, its application to the Venturi geometry as well as the flow conditions were repeatable.

4 Relationship between the cavitation structures and erosion

We investigated three parameters that could form a relationship to the damage extent: the distance of the cloud from the foil at its collapse, the volume of the cloud and the structure of the cloud just before the collapse.

The distance of the cloud collapse from the wall could be easily measured from the side view image of cavitation cloud just before it collapses.

The volume of the bubble cloud at the instant when it separates from the attached part of the cavity could only be approximated as we did not measure the void fraction. From the side view images we determined the boundary of the cloud and measured its area. In the present experiment the clouds are in essence two dimensional what can be seen from the top view images (Fig. 13). The approximate could volume can then be easily determined by multiplying the area by the width of the channel (10 mm).

Results that show the relationship between the damaged area caused by a specific cloud collapse, the distance of the cloud from the foil at its collapse and the volume of the cloud size at its separation from the attached cavity are presented in Fig. 14.

We can see that neither the distance at which the cloud collapses nor the volume of the cloud play a significant role for the erosion process. This is somewhat unexpected – for example Dular et al. [17] included the distance of the cloud collapse in his cavitation erosion model. Similarly Preira et al. [9] reports that the volume of the cavitation cloud significantly influences the aggressiveness of cavitation erosion.

We hypothesize that the reason for not finding a clear relationship between the distance of the cloud collapse and the damaged volume, is a result of the nature of how the shock wave, which is emitted at cloud collapse, is attenuated. Its magnitude decreases exponentially by the distance it travels [17], but since the compressibility of the water is very low it remains practically unchanged regardless the distance that it traveled (2 or 12 mm).

From the work of Wang & Brennen [4] one can conclude that collapses of larger cavitation clouds with the same inner structure should produce shock waves with higher magnitude, consequently causing more damage to the surface of the Venturi section. The reason that we did not find this straightforward relationship lies in the fact that, as already mentioned, the cavitation erosion process is made out of a sequence (cascade) of events. The shock wave that is emitted at cloud collapse does not damage the surface directly – it influences the individual bubbles that are in the vicinity the wall, which then implode and form a pit. It seems that the number and the distribution of the single bubbles in the vicinity of the wall have a mayor role in the process of cavitation erosion.
Another possible explanation was recently suggested by van Rijsbergen et al. [34]. Based on acoustic emission measurements they came to a similar conclusion – that not all cloud implosions lead to impacts on the nearby surface. They hypothesize that, that the shock waves are not perfectly spherical and have a clear orientation – the highest impact occurs when the wave front is directed toward the wall.

Finally we investigated the structure of the cloud 0.33 ms prior to its collapse. Figure 15 shows three images of the clouds which caused small damage (left) and three which caused extensive damage (right). The value of the area, which is written in the images corresponds damage that the foil sustained from this specific cloud collapse.

We see that the clouds that caused extensive erosion appear to be “broken” and asymmetrical. We believe that the “broken” structure of the cloud causes shedding of many individual bubbles which can later cause the damage to the material (according to the cascade approach). When the clouds are symmetrical (round shaped) as the ones in the left column in Fig. 15 the collapse may be more violent but there are simply not enough single bubbles in the vicinity of the wall which could damage the material. This again proves that it is the number and the distribution of the single bubbles which is the most influential parameter in the process of cavitation erosion.

4 Conclusions

A study of simultaneous observations of cavitation structures and cavitation erosion was presented. By using a thin aluminum foil, which we observed from the side which was not exposed to cavitation we were able to relate individual cavitation cloud collapses to individual cavitation erosion pits that formed on the foil.
The most important conclusions that can be drawn from the study are:

1. Cavitation cloud collapse is evidently the needed condition for cavitation damage occurrence – no erosion was found during the period of cavitation growth and separation. The cavitation cloud shedding, however, does not need to be strictly periodic for cavitation to be aggressive [9].
2. Provided that the cavitation cloud collapse occurs, the distance of the cloud from the foil at its collapse and the volume of the cloud do not influence the extent of the damage.
3. It is the topology of the cloud just before its collapse that plays a major part in the process of erosion.
4. The cascade approach to the explanation of cavitation erosion process is valid.

There are two possible explanations to why an irregular (non circular) or "broken" cavitation cloud causes more erosion. It either sheds more individual bubbles which later on implode and cause more extensive damage or, according to van Rijsbergen et al. [34], it influences the orientation of the shock wave which turns toward the surface.

References

[1] L. Rayleigh, On the pressure developed in a liquid during the collapse of a spherical cavity, Philos. Mag. 34, 1917, pp. 94–98.

[2] J.P. Franc, J.M. Michel, Fundamentals of Cavitation, Kluwer Academic Publishers, 2004.

[3] F. G. Hammitt, Observations on Cavitation Damage in a Flowing System", Trans. ASME, J. of Basic Engineering, 1963, pp. 3.

[4] Y. C. Wang, C.E. Brennen, Shock wave development in the collapse of a cloud of bubbles, FED Vol 194, Cavitation and Multiphase flow, ASME 1994.

[5] Y.L. Chen, J. Israelachvili J, New mechanism of cavitation damage. Science 252, 1991, pp. 1157-1160.

[6] T.J.C. Van Terwisga , P.A. Fitzsimmons , L. Ziru, E.J. Foeth, Cavitation Erosion – A review of physical mechanisms and erosion risk models, Proceedings of the 7 International Symposium on Cavitation CAV2009 – Paper No. 41 August 17-22, 2009, Ann Arbor, Michigan, USA.

[7] R. Fortes-Patella, J.L. Reboud, L. Briancon-Marjollet, A phenomenological and numerical model for scaling the flow aggressiveness in cavitation erosion, EROCAV Workshop, Val de Reuil, 2004.

[8] G. Bark, J. Friesch, G. Kuiper, J.T. Ligtelijn, Cavitation Erosion on Ship Propellers and Rudders, 9th Symposium on Practical Design of Ships and Other Floating Structures, Luebeck-Travemuende, Germany, 2004.

[9] Pereira , F., Avellan, F., and Dupont, J.M., 1998, "Prediction of Cavitation Erosion: an Energy Approach", Journal of Fluid Engineering, Transactions of the ASME, Vol. 120, December 1998

[10] G.E. Reisman, Y.C. Wang, C.E. Brennen, Observations of shock waves in cloud cavitation, Journal of Fluid Mechanics, 355, 1998, pp. 255-283.

[11] M. Dular, B. Bachert, B. Stoffel, B. Sirok, Relationship between cavitation structures and

cavitation damage, Wear 257, 2004, pp. 1176–1184.

[12] M. Gavaises, D. Papoulias, A. Andriotis, E. Giannadakis, Link between cavitation development and erosion damage in diesel injector nozzles", Congress on Diesel Fuel Injection and Sprays (SP-2083), SAE International, 2007.

[13] G. Bark , M. Grekula, R.E. Bensow , N. Berchiche, On some physics to consider in numerical simulation of erosive cavitation, Proceedings of the 7 International Symposium on Cavitation, CAV2009 – Paper No. 41 August 17-22, 2009, Ann Arbor, Michigan, USA.

[14] B. Belahadji, J.P. Franc, J.M. Michel, A Statistical Analysis of Cavitation Erosion Pits, ASME J. Fluids Eng., 113, 1991, pp. 700–706.

[15] H. Kato, A. Konno, M. Maeda, H. Yamaguchi, Possibility of Quantitative Prediction of Cavitation Erosion Without Model Test", ASME J. Fluids Eng., 118, 1996, pp. 582-588.

[16] G. Bark, N. Berchiche, M. Grekula, Application of principles for observation and analysis of eroding cavitation – The EROCAV observation handbook", Edition 3.1, 2004.

[17] M. Dular, B. Stoffel, B. Sirok, Development of a cavitation erosion model. Wear 261(5–6), 2006, pp. 642–655.

[18] P. Zima, M. Sedlář , M. Müller, Modeling collapse aggressiveness of cavitation bubbles in hydromachinery , Proceedings of the 7 International Symposium on Cavitation CAV2009 – Paper No. 41 August 17-22, 2009, Ann Arbor, Michigan, USA.

[19] M. Dular, O. Coutier-Delgosha , Numerical modelling of cavitation erosion nt. J. Numer. Meth. Fluids, 61, 2009, pp. 1388–1410 .

[20] S., Lang, M., Dimitrov, P.F., Pelz, Spatial and temporal high resolution measurement of bubble impacts, Proceedings of the 8th International Symposium on Cavitation CAV2012, - paper no. 210, August 13-16, 2012, Singapore.

[21] R.T., Knapp, Recent investigations of the mechanics of cavitation and cavitation damage, Trans. ASME 75 (8), 1955, pp. 1045–1054.

[22] Y., Ito, R., Oba, Comparison between four practical methods to detect the erosive area in cavitating flows, in: Proceedings of the XVII IAHR Symposium, 1994, Beijing.

[23] R., Simoneau, Cavitation pit counting and steady state erosion rate, Proceedings of the International Symposium on Cavitation CAV95, 1995, Deauville.

[24] S., Lavigne, A., Retailleau, J., Woillez, Measurement of the aggressivity of erosive cavitating flows by a technique of pits analysis. Application to a method of prediction of erosion, Proceedings of the International Symposium on Cavitation CAV95, 1995, Deauville.

[25] X. Escaler, M. Farhat, F. Avellan, E. Egusquiza, Cavitation erosion tests on a 2D hydrofoil using a surface-mounted obstacles, Wear 254, 2003, pp. 441–449.

[26] M. Dular, B. Sirok, B. Stoffel, Influence of gas content in water and flow velocity on cavitation erosion aggressiveness. Journal of Mechanical Engineering, 51, 2005, pp. 132–145.

[27] F. Brand, Ein physikalisches Verfahren zur Bestimmung von geloesten und ungeloesten Gasen in Wasser, Voith Forschung und Konstruktion, Vol. 27, 1981.

[28] F.B. Peterson, Hydrodynamic cavitation and some considerations of the influence of free gas content, 9th Symp. on Naval Hydrodynamics, 1972.

[29] R.E.A. Arndt, A.P. Keller, Free gas content effects on cavitation inception and noise in a free shear flow, IAHR Symp. Two Phase Flow and Cavitation in Power Generation Systems, Grenoble, 1976.

[30] H. Lohrberg, M. Hofmann, G. Ludwig, B. Stoffel, Analysis of Damaged Surfaces: Part II: Pit Counting by 2D Optical Techniques. Proceedings of the 3rd ASME / JSME Joint Fluids Engineering Conference, San Francisco CA, 1999 .

[31] M. Dular, A. Osterman, Pit clustering in cavitation erosion. Wear, 265, 2008, pp. 811–820.

[32] T. Keil, P. F. Pelz, U. Cordes, G. Ludwig, Cloud Cavitation and Cavitation Erosion in Convergent Divergent Nozzle , WIMRC 3rd International Cavitation Forum 2011 University of Warwick, UK, 4th-6th July 2011.

[33] A. Osterman, B. Bachert, B. Sirok, M. Dular, Time dependant measurements of cavitation damage. Wear, 266, 2009, pp. 945–951.

[34] M., van Rijsbergen, E.J., Foeth, P., Fitzsimmons, A., Boorsma, High speed video observations and acoustic impact measurements on a NACA0015 foil, Proceedings of the 8th International Symposium on Cavitation CAV2012, - paper no. 280, August 13-16, 2012, Singapore.

Figure captions

Fig. 1: The Venturi geometry and the directions of observation.

Fig. 2: The experimental setup. (1) Pump, (2) upstream tank, (3) test section, (4) downstream tank, (5 and 6) valves, (7) electromagnetic flow meter (7), (8) thermocouple, (9) pressure sensor, (10) compressor and (11) vacuum pump.

Fig. 3: The evolution of the mean cavitation length during the experiment. t=0 s corresponds to the first appearance of cavitation.

Fig. 4: The foil applied to the Venturi section.

Fig. 5: Image of cavitation and the foil in respect to the position of the Venturi.

Fig. 6: Manipulation of the images of the damaged surface. From each image pair we obtained the number and the area of newly appeared pits (at $t+\Delta t$).

Fig. 7: Instantaneous image of the aluminum foil (top images), measured damage of the foil up to this instant (middle images) and instantaneous image of cavitation (bottom images).

Fig. 8: The damage after every 0.1 s exposure to cavitation.

Fig. 9: The number of pits and integral damage extent as a function of time. Left - the whole length of the experiment, right - a short time interval during the experiment (with noted instances of cavitation cloud collapse).

Fig. 10: Average area of the pit during the experiment (left) and histograms of pit size distribution (middle) and the contribution to the whole damaged area of the pits of a specific size (right).

Fig. 11: Number of deformations that formed a single pit as seen by the end of the experiment.

Fig. 12: Study of the repeatability of the experiments: The integral damage extent as a function of time

(left), damage extent after 0.8 s exposure to cavitation (right).

Fig. 13: Determining the volume of the cavitation cloud.

Fig. 14: Relationship between the damaged area caused by the cloud collapse, the distance of the cloud from the foil at its collapse and the volume of the cloud size at its separation from the attached cavity.

Fig. 15: Cavitation clouds 0.33 ms prior to the collapse with noted damage extents. Small damage (left) extensive damage (right).

Highlights

- We simultaneously recorded cavity collapse and damage occurrence
- The distance of the cloud at its collapse does not influence the extent of the damage.
- The volume of the cloud does not influence the extent of the damage.
- Erosion significantly depends on the topology of the cloud just before its collapse.
- The cascade approach to the explanation of cavitation erosion process is valid.

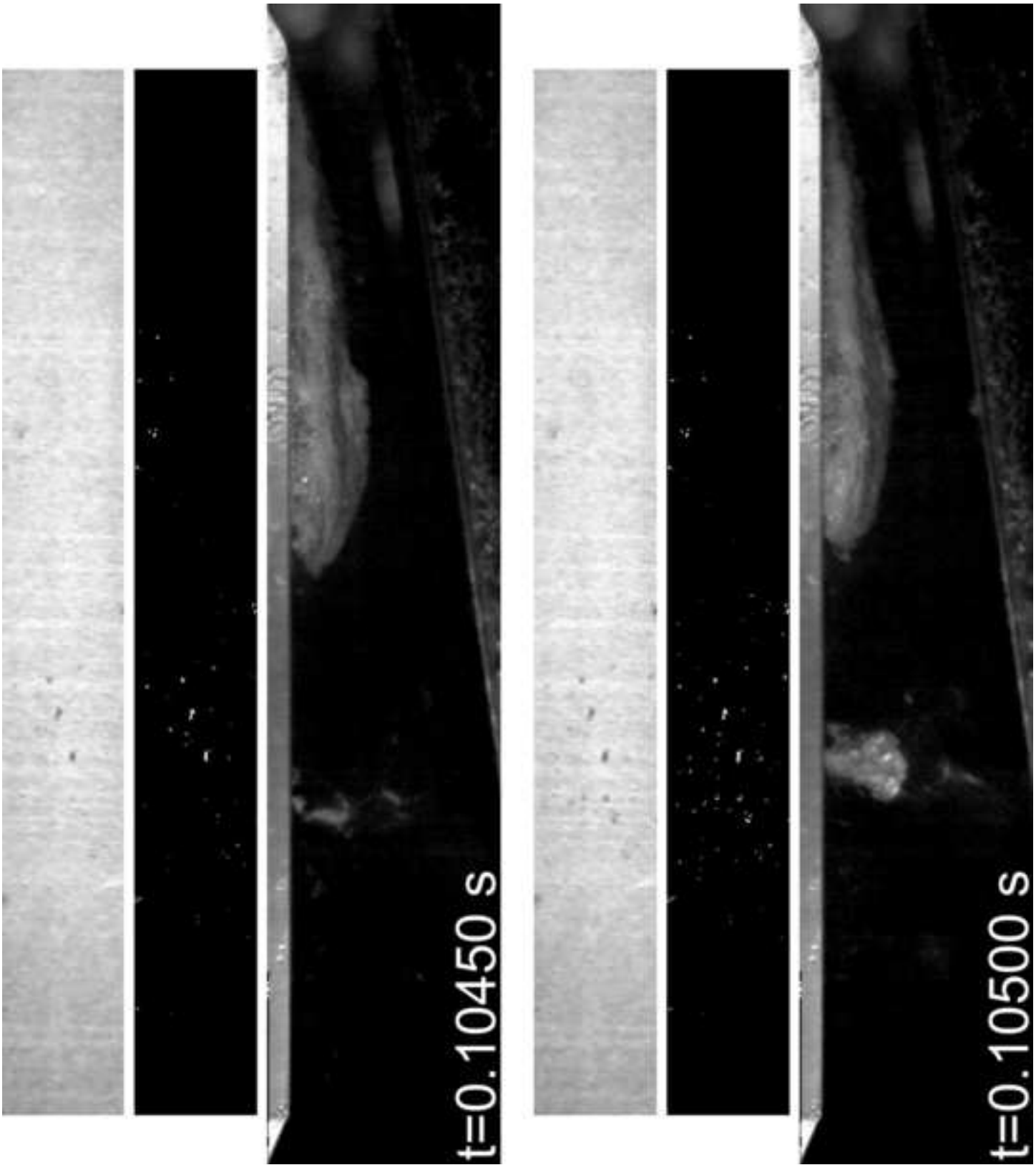

Graphical Abstract (for review)

Figure15

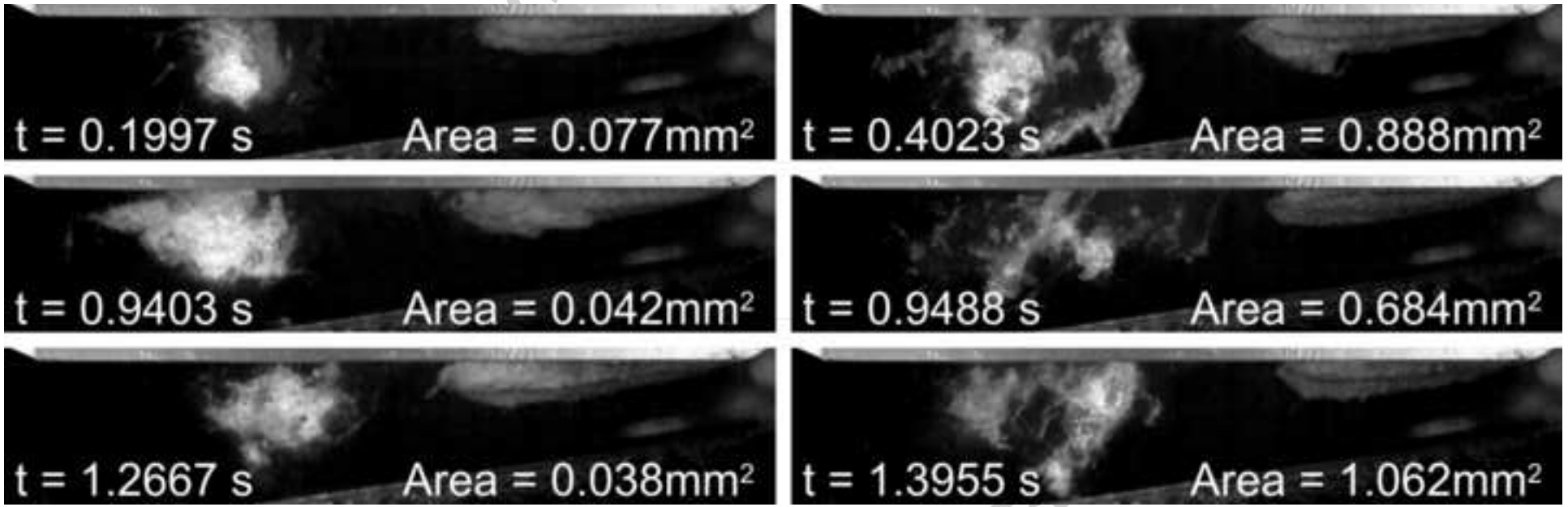

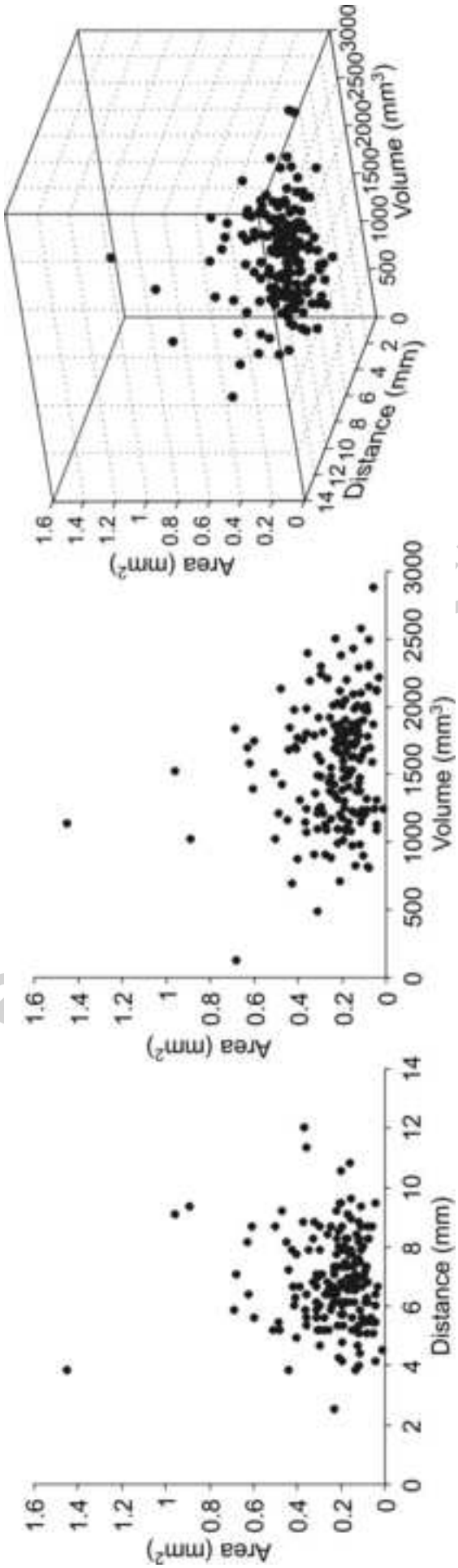
Area (mm²)
Distance (mm)
Volume (mm³)
0
0.2
0.4
0.6
0.8
1
1.2
1.4
1.6
2
4
6
8
10
12
14
500
1000
1500
2000
2500
3000

Figure14

Figure13

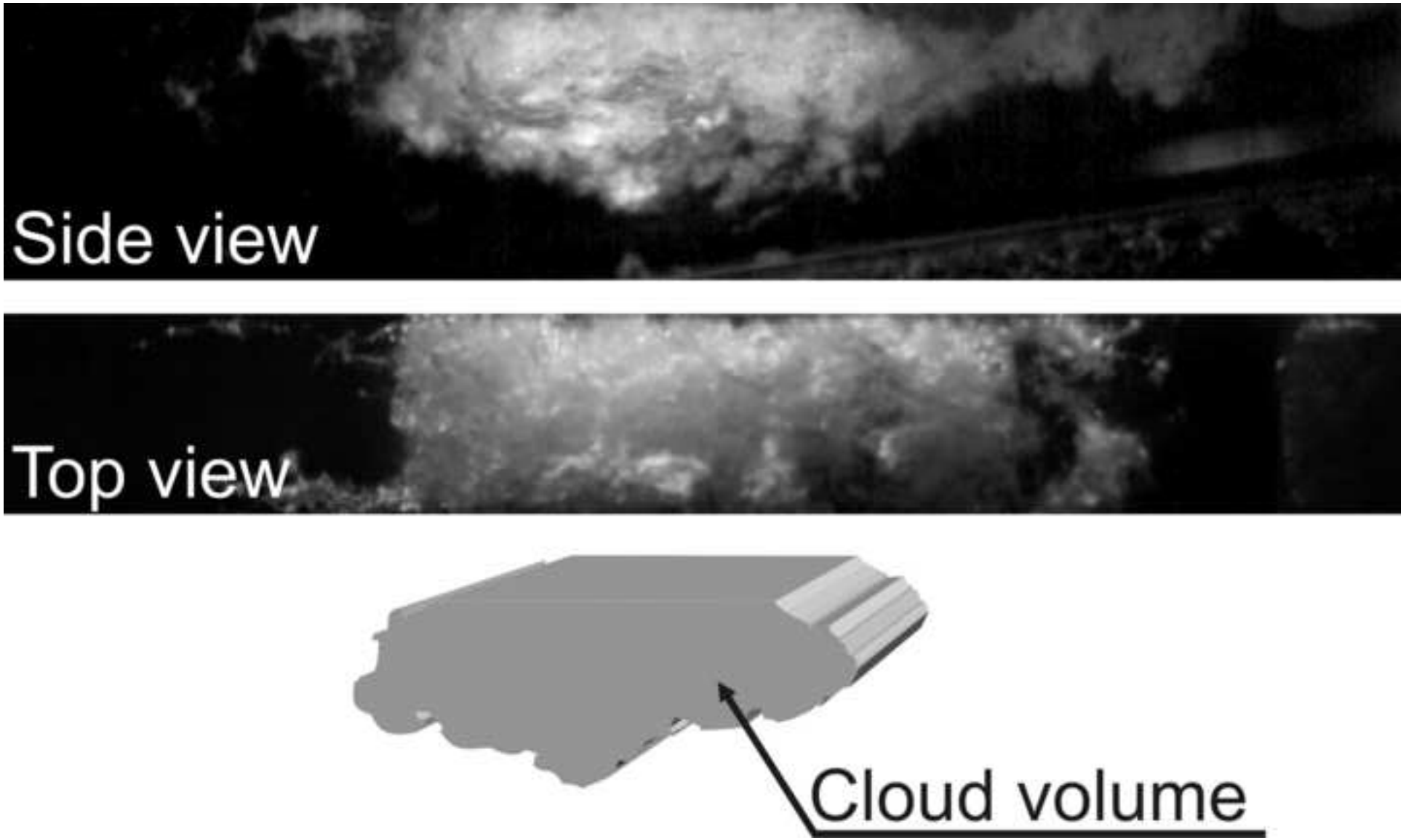

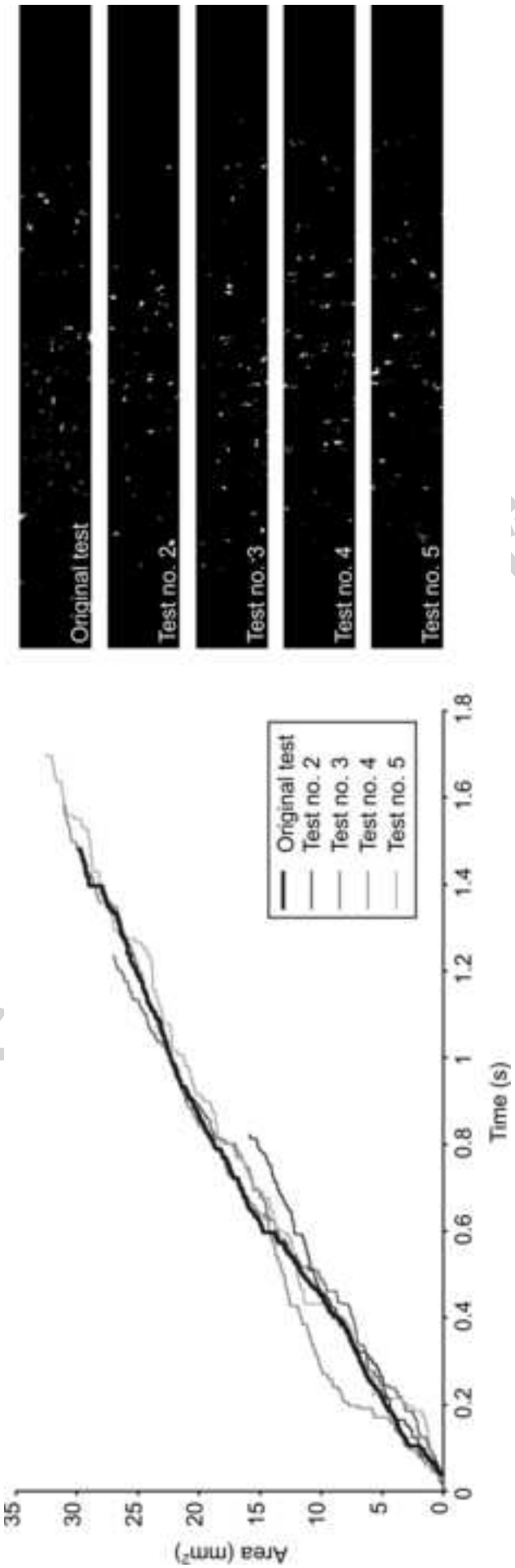
Original test
Test no. 2
Test no. 3
Test no. 4
Test no. 5
Original test
Test no. 2
Test no. 3
Test no. 4
Test no. 5
Area (mm²)
Time (s)
0
5
10
15
20
25
30
35
0
0.2
0.4
0.6
0.8
1
1.2
1.4
1.6
1.8

Figure12

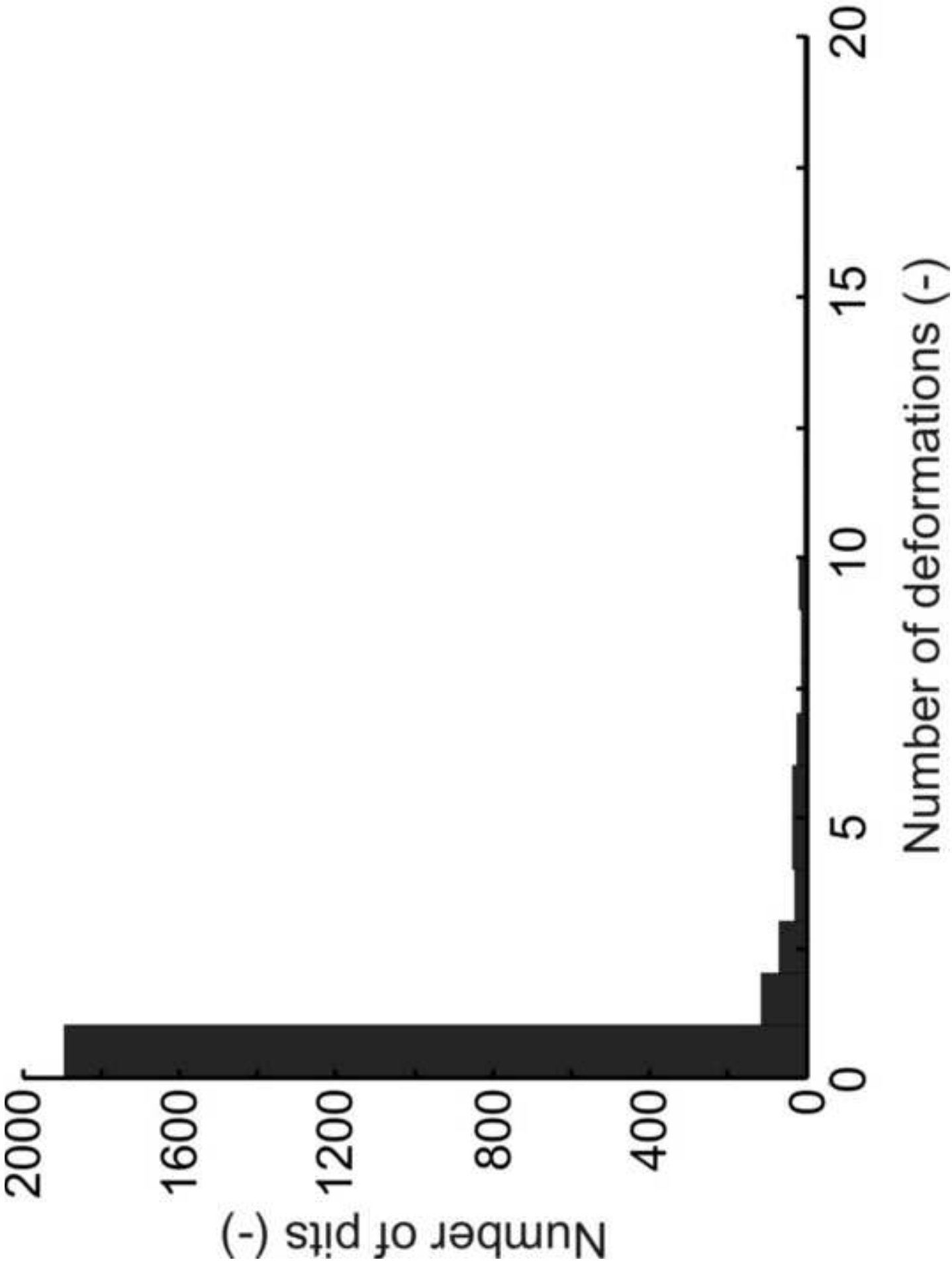
Number of pits (-)
2000
1600
1200
800
400
0
0
5
10
15
20
Number of deformations (-)

Figure11

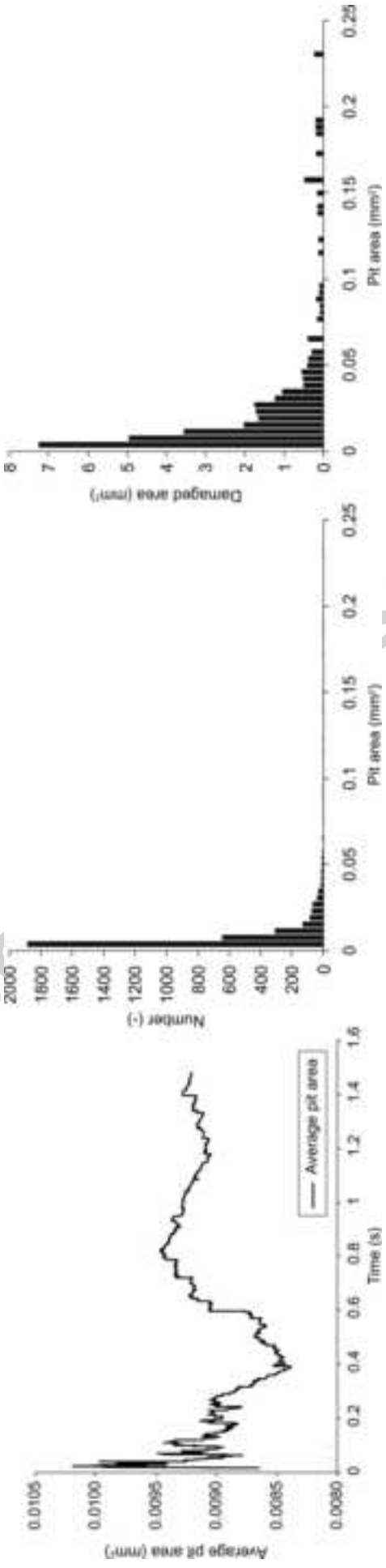
Damaged area (mm²)
Pit area (mm²)
Number (-)
Pit area (mm²)
Average pit area
Time (s)
Average pit area (mm²)

Figure10

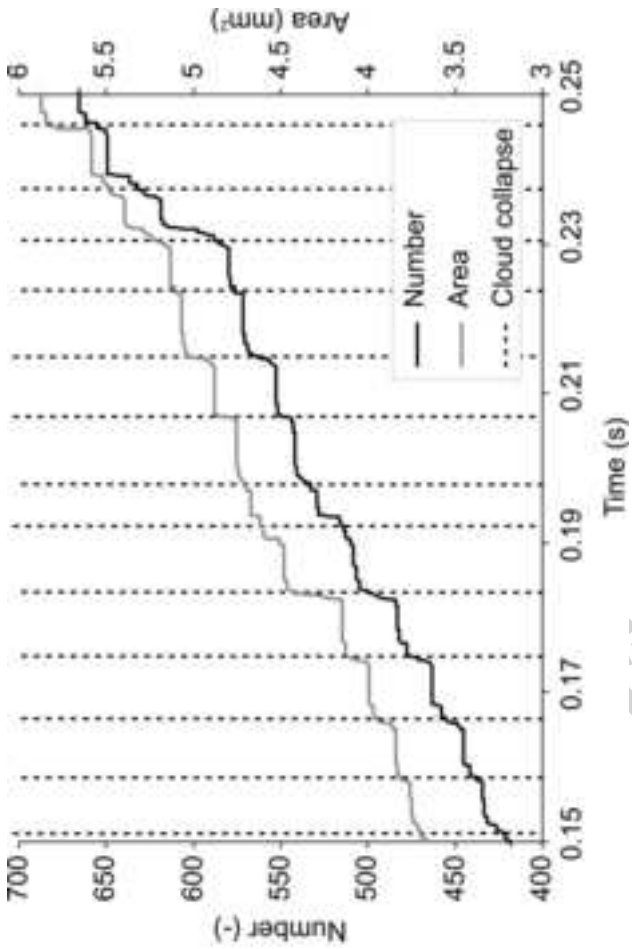

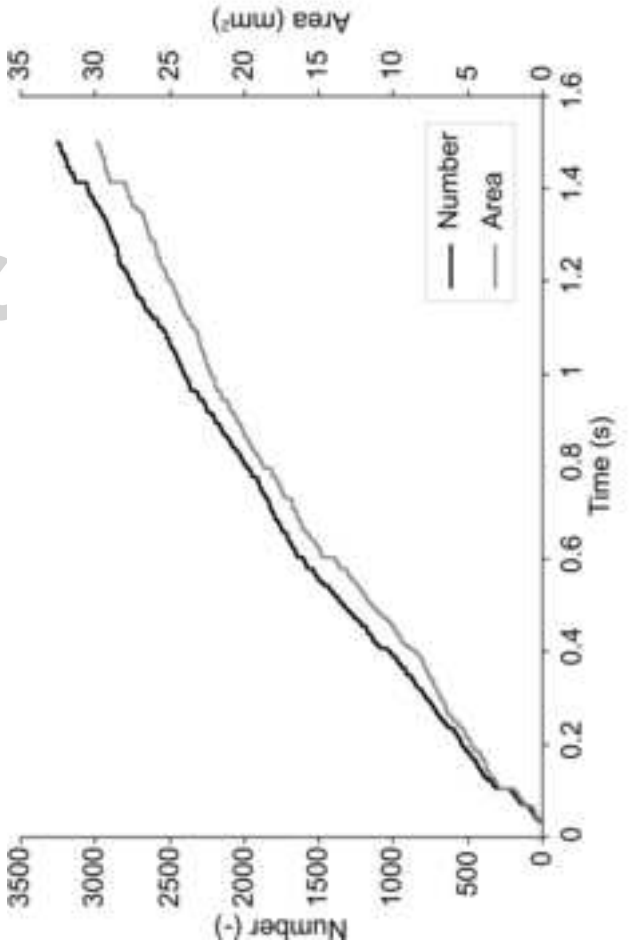

Figure09

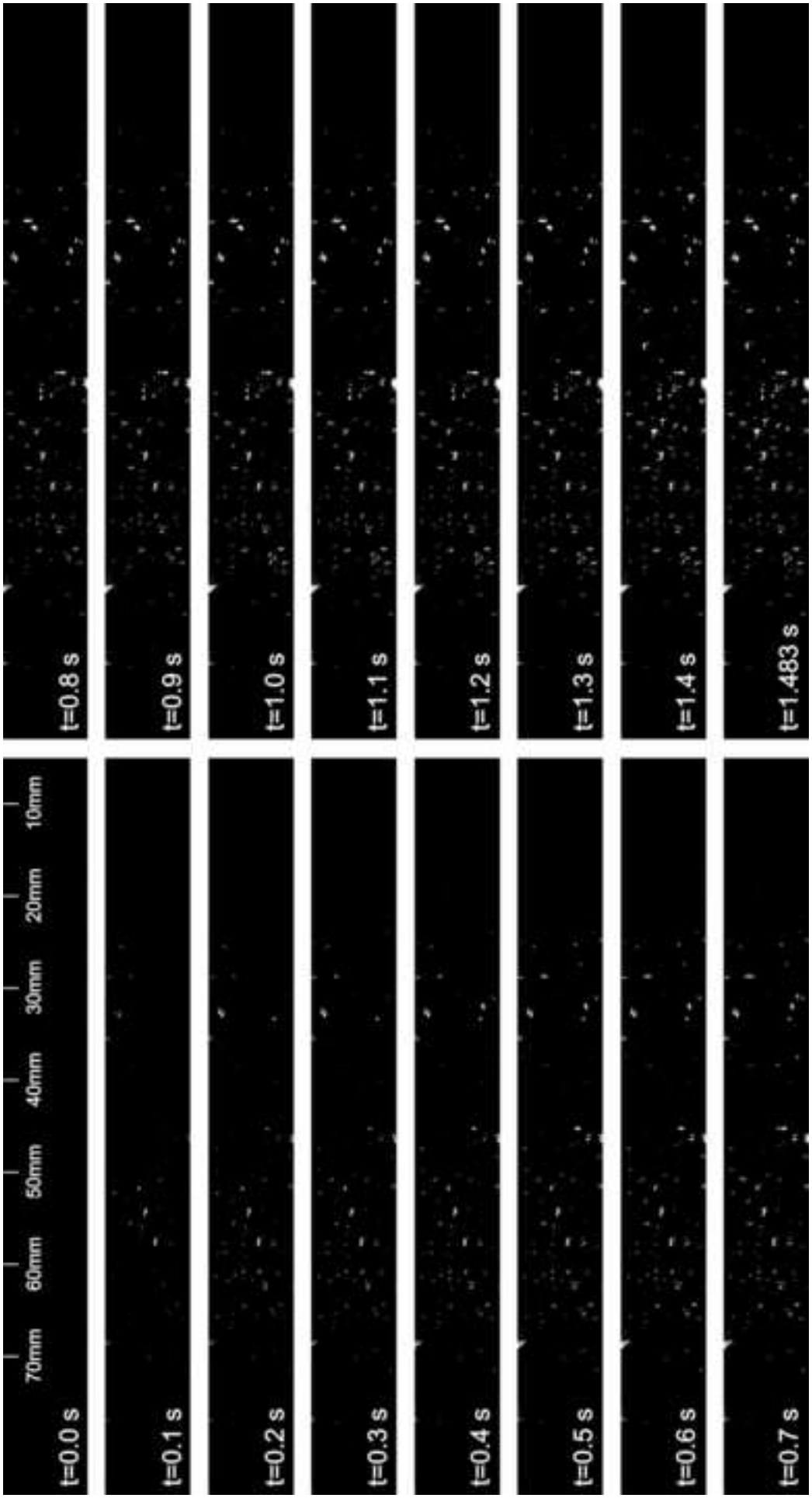
70mm
60mm
50mm
40mm
30mm
20mm
10mm
t=0.0 s
t=0.1 s
t=0.2 s
t=0.3 s
t=0.4 s
t=0.5 s
t=0.6 s
t=0.7 s
t=0.8 s
t=0.9 s
t=1.0 s
t=1.1 s
t=1.2 s
t=1.3 s
t=1.4 s
t=1.483 s

Figure08

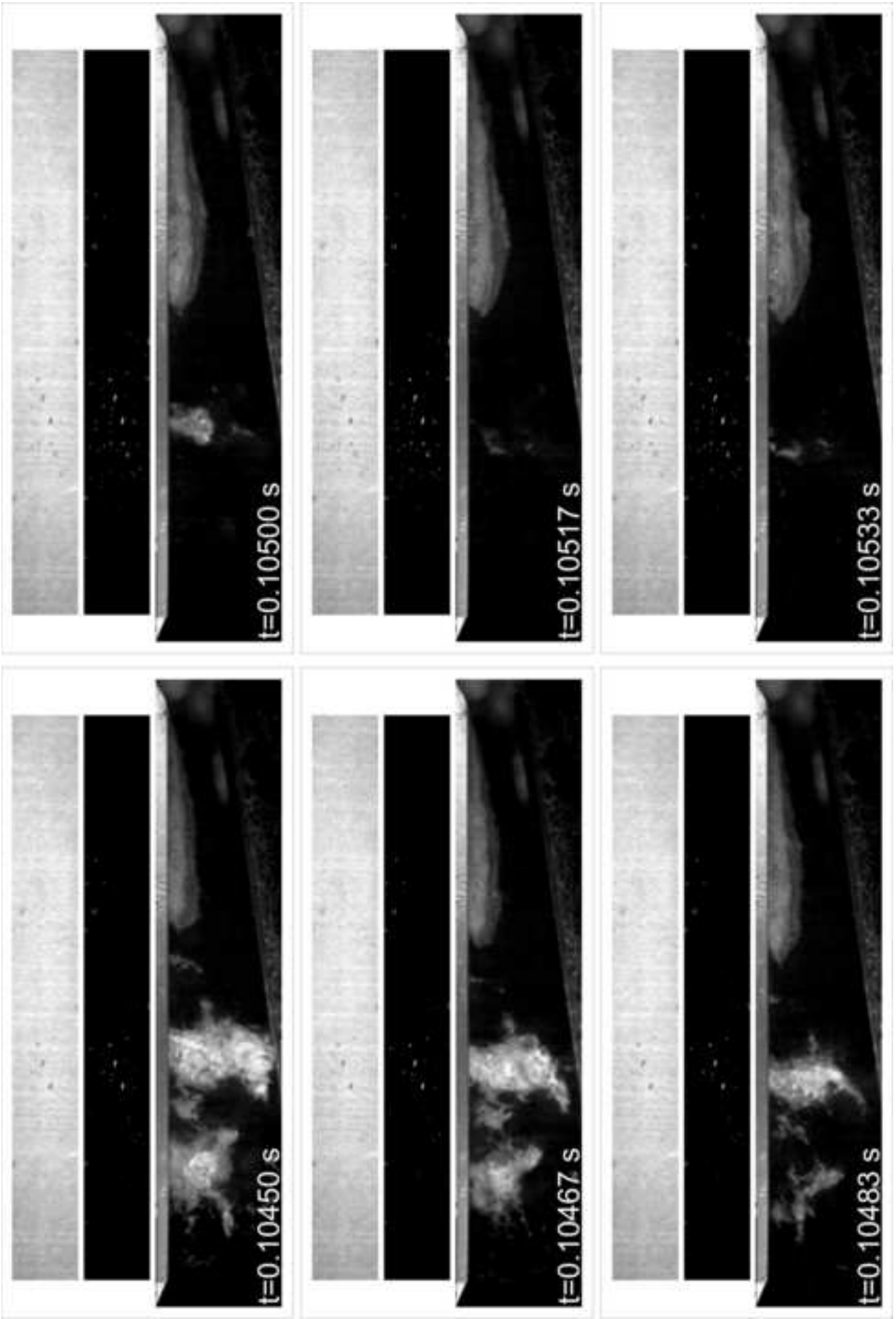

Figure07

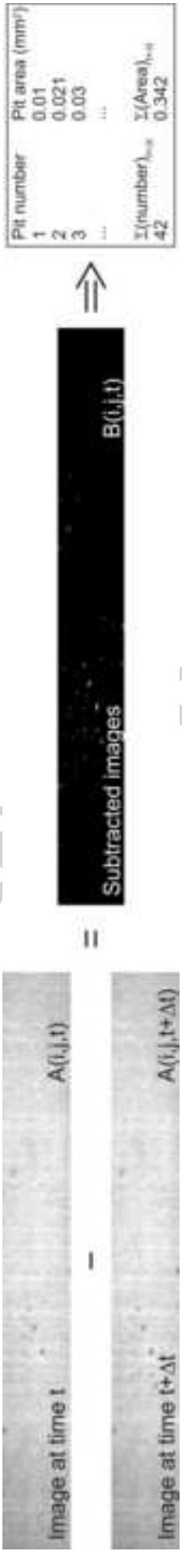

Figure06

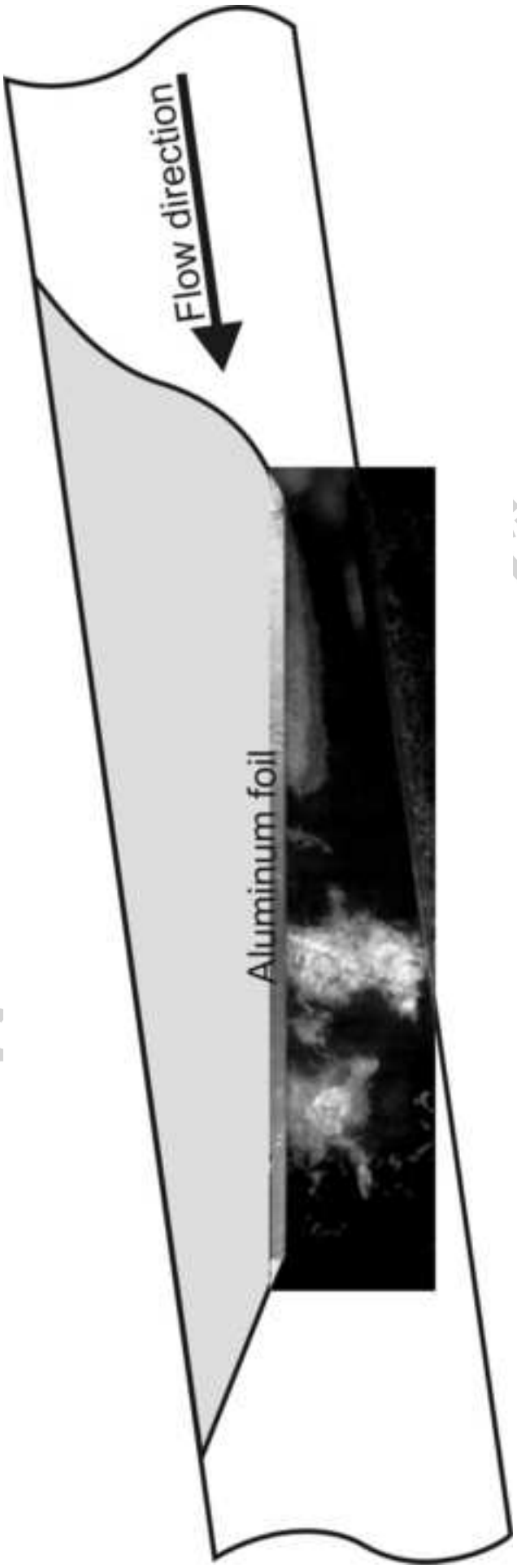

Figure05

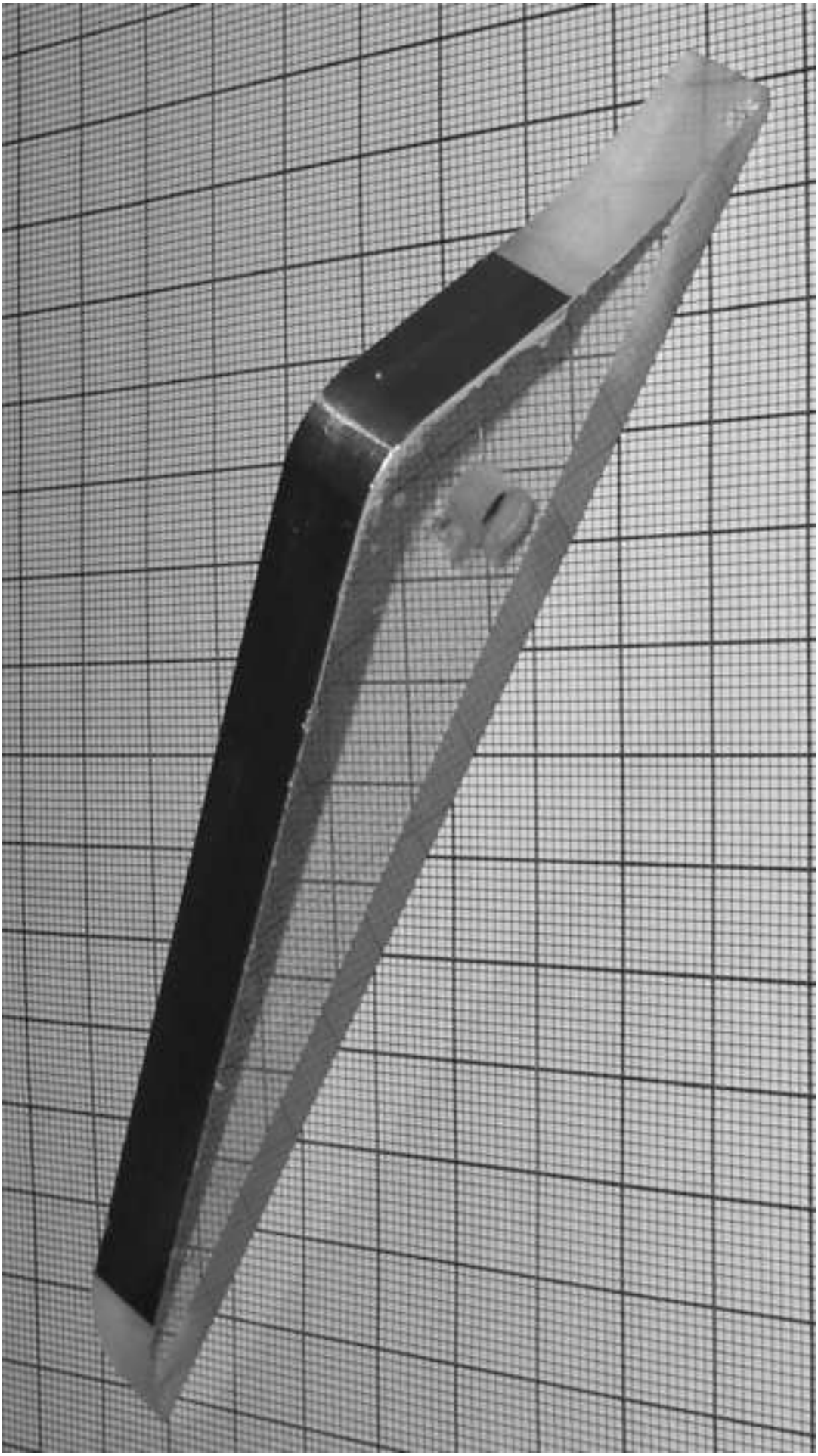

Figure04

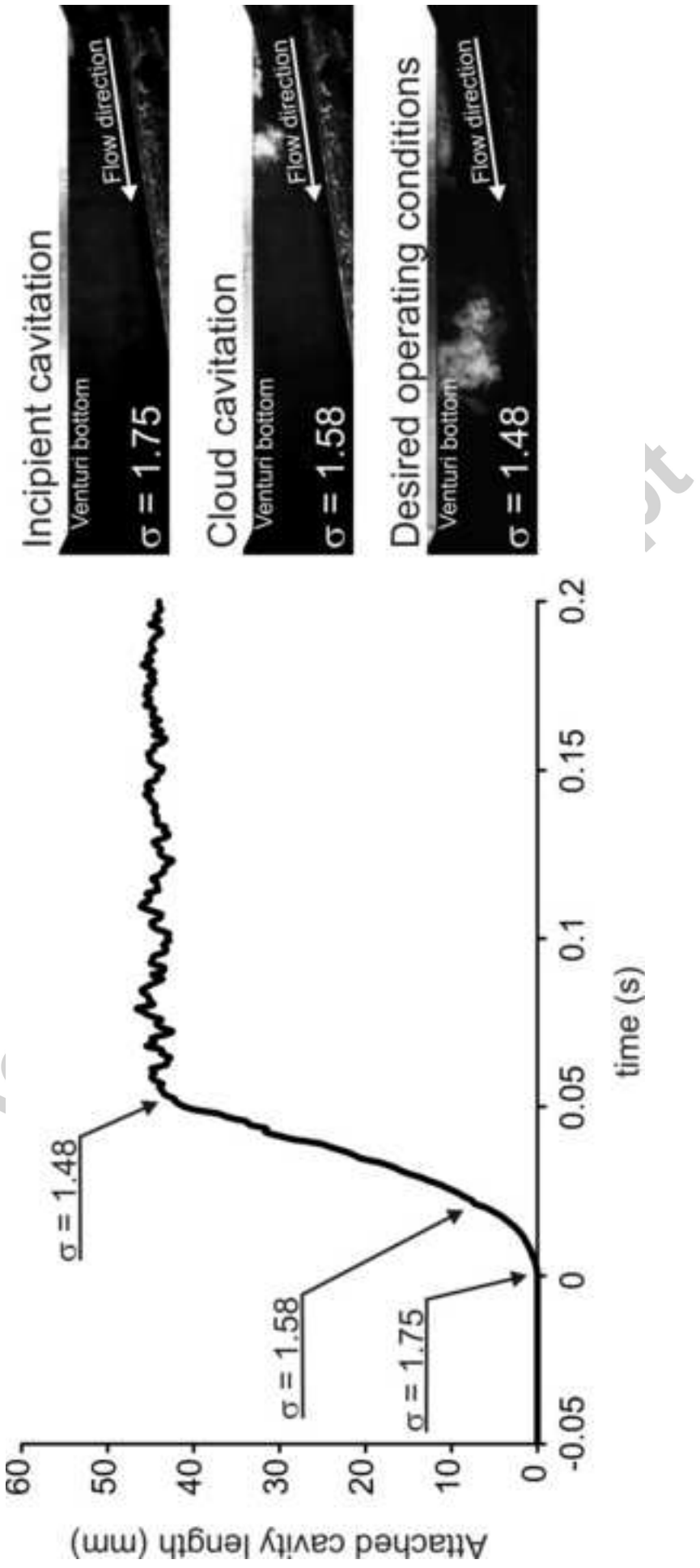
Incipient cavitation
Venturi bottom
Flow direction
σ = 1.75
Cloud cavitation
Venturi bottom
Flow direction
σ = 1.58
Desired operating conditions
Venturi bottom
Flow direction
σ = 1.48
Attached cavity length (mm)
60
50
40
30
20
10
0
-0.05
0
0.05
0.1
0.15
0.2
time (s)
σ = 1.48
σ = 1.58
σ = 1.75

Figure03

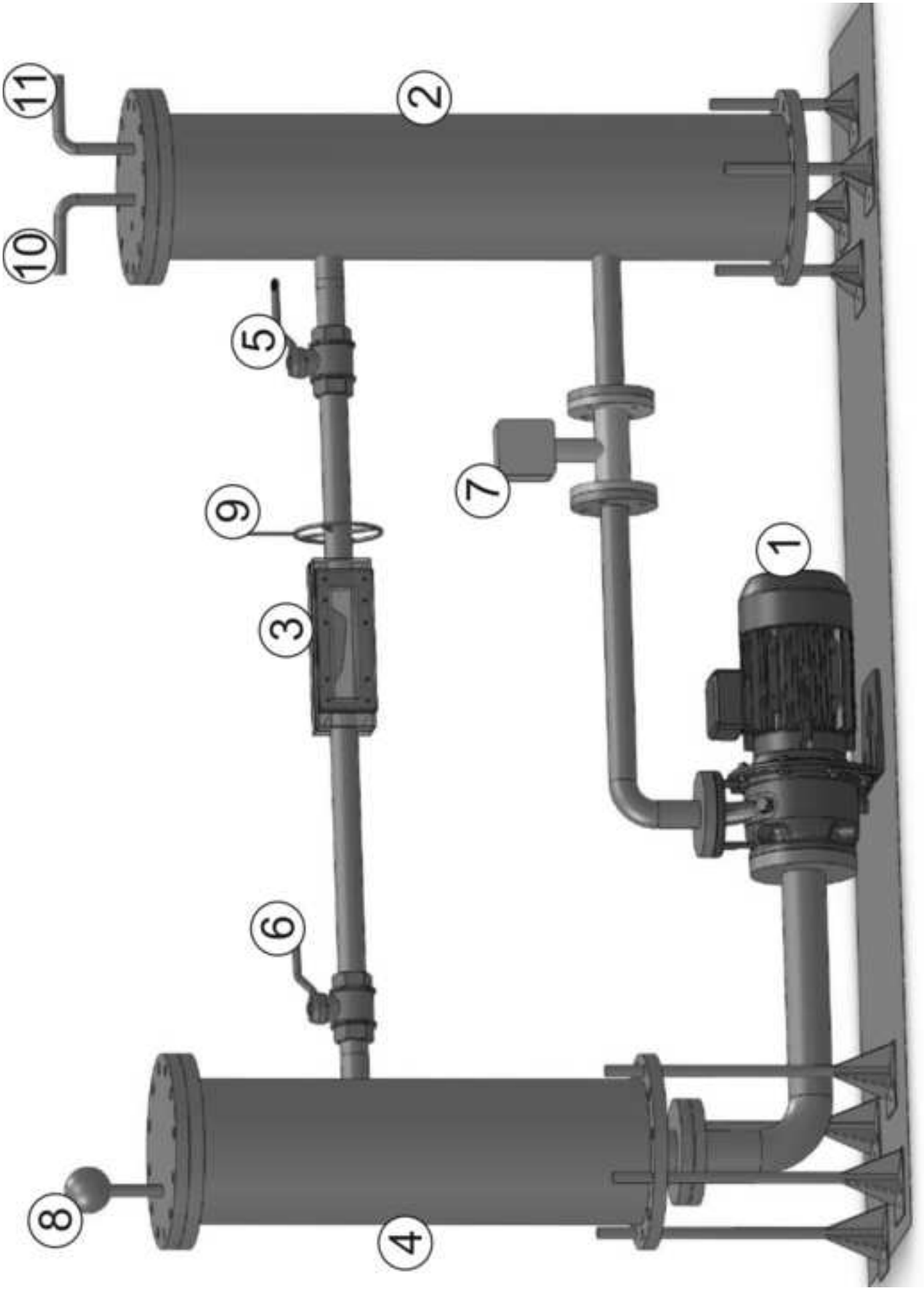

Figure02

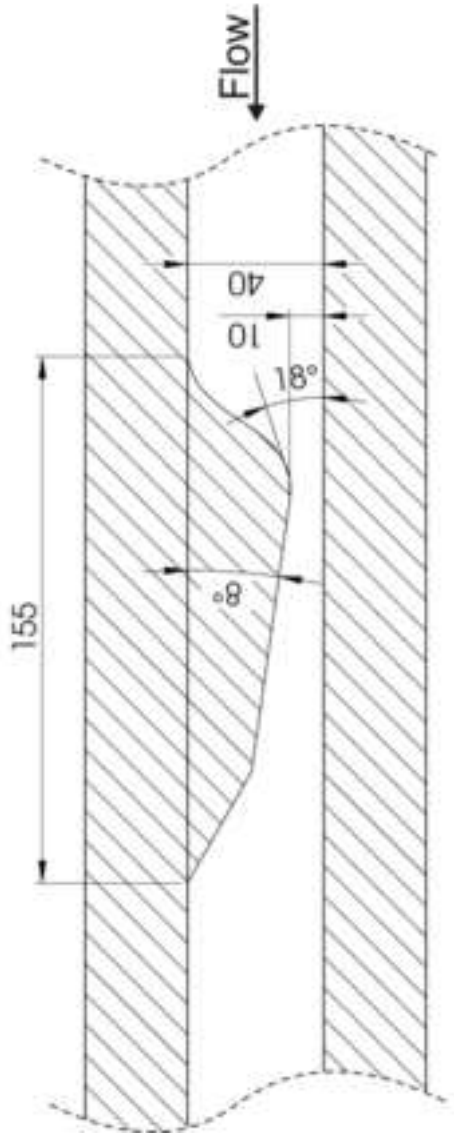

Figure01